25th International Congress on Modelling and Simulation, Darwin, NT, Australia, 9 to 14 July 2023
mssanz.org.au/modsim2023

A computational framework for phenomenological modelling of ember storms at the wildland-urban interface

T. M. Saurav [a], **D. Sutherland** [a] **and J. Sharples** [abc]

[a] *School of Science, The University of New South Wales, Canberra ACT 2610*
[b] *ARC Centre of Excellence for Climate Extremes, UNSW Canberra ACT 2610*
[c] *NSW Bushfire and Natural Hazards Research Centre*
Email: t.saurav@adfa.edu.au

Abstract: Bushfires are a frequent occurrence in Australia that cause significant property damage, loss of wildlife, and human lives. To ensure resilience of structures and urban developments in Australia, Australian Standard AS3959 (Standards Australia 2018) sets construction requirements for houses in bushfire-prone areas. The model used to estimate the risk to a property is exclusively based on the radiative heat load received at the property from an idealised fire (Douglas & Tan 2005, Roberts et al. 2017). This, however, does not directly consider the risk posed by other bushfire attack mechanisms. For example, burning vegetation creates embers, which are transported significant distances from the main fire front by wind and can create secondary ignitions based on the availability of nearby fuels. This process is known as 'spotting' and has been identified as the leading cause of house loss in previous fire events (Blanchi & Leonard 2005).

Near the wildland-urban interface (WUI), embers can cross fire lines and flow into properties, creating structure damage. Several experimental and computational studies have investigated ember transportation (e.g., Manzello et al. (2020)). However, these studies have considered embers to be 'ballistic' in nature, where the embers get entrained into the air and travel significant distance while airborne. 'Ember storms', on the other hand, are characterised by the embers sliding across the ground and being repeatedly lofted into the air. This near ground behaviour is not captured by any current models, which restricts their capacity to inform accurate policy decisions.

This paper describes a computational framework that incorporates several components of the WUI with adjustable parameters, including forest density, wind speed, and building spacing, that can be used to simulate an ember storm. The popular spectral element method (SEM) solver 'Nek5000' has been used to perform large-eddy simulation of flow through a forest canopy towards an idealised urban canopy represented by an array of cubes. A Lagrangian particle transport model was implemented using an external particle library 'ppiclF'. Embers were lofted into the air using a phenomenological lifting model. The framework showed great potential in simulating ember storms and can be used for further parametric studies to investigate the onset of ember storms at the WUI. This will help ensure that authorities are better equipped to deal with wildfires at the WUI and formulate better mitigation strategies.

Keywords: *Bushfire, computational fluid dynamics, large-eddy simulation, embers*

1 INTRODUCTION

Bushfires are a frequent occurrence in Australia, however, fire frequency and fire intensity are increasing as a result of climate change (Jolly et al. 2015). The 2009 bushfires in south-eastern Australia burned over 450,000 ha and took 173 human lives (Cruz et al. 2012). The recent 2019-2020 fire season in New South Wales cost 26 lives due to the direct impact of fires, burned 5.5 million hectares, and caused infrastructure and telecommunication site losses of AUD942 million (Owens & O'Kane 2020). A greater potential for damage is at the wildland-urban interfaces (WUI) (Figure 1), areas where structures and developments meet wildland. Burning vegetation creates embers, which can be transported significant distances from the main fire front by wind and can create a secondary ignition ('spotting') based on the availability of nearby fuels. Spotting has been identified as the leading cause of house loss in previous fire events (Blanchi & Leonard 2005). Near WUI areas, embers pose a greater risk as small ember particles can flow over roads and terrain into properties, increasing the likelihood of structure damage.

Figure 1. An example of a wildland-urban interface (WUI) in the outer suburbs of Sydney. (Source: Google Maps).

The existing literature has almost exclusively considered embers to follow a single trajectory from when they are entrained into the flow to when they encounter an obstacle or fall to the ground (Manzello et al. 2020). This type of ember can be termed 'ballistic'. However, anecdotal and video evidence (Figure 2) have shown millimetre-scale embers that slide (creep) over the ground before they are lofted one to two metres high, and they may fall to the ground before being relofted; a phenomenon termed as an 'ember storm' (McRae 2010). Near WUIs, ember storms can easily cross fire control lines or enter structures and create spotfires in habitable areas. Existing computational models do not capture the near-ground behaviour and transportation of embers, and the entrainment (the process through which near-ground particles are introduced into the flow) of embers from the ground, both of which are key factors in ember storms. Thus, a computational model of ember storms is necessary to reform the design of safer WUIs for future development, and offer better mitigation strategies at current WUIs. Computational models offer cost-effective, fast, and reliable prediction of fire behaviours.

2 COMPUTATIONAL MODELLING

Problems that involve fluid flows, such as the behaviour of wind, the spread of bushfires, and respiratory and cardiovascular systems, can be simulated using computational fluid dynamics (CFD). It is a branch of fluid mechanics that uses numerical methods to solve the governing equations of fluid motion, known as the Navier–Stokes equations. For an incompressible, Newtonian fluid, these equations are written as,

$$\nabla \cdot \mathbf{u} = 0 \quad \text{(Continuity)} \tag{1}$$

$$\frac{\partial \mathbf{u}}{\partial t} + (\mathbf{u} \cdot \nabla)\,\mathbf{u} = -\frac{1}{\rho}\nabla p + \nu \nabla^2 \mathbf{u} + \frac{1}{\rho}\mathbf{F} \quad \text{(Momentum)} \tag{2}$$

Figure 2. Still frame taken from a video of an ember storm (*Ember attack during bushfire on the Sunshine Coast* 2019). Red glowing embers can be seen sliding aand bouncing along the ground.

with prescribed boundary and initial conditions, where ρ is the density of the fluid, $\mathbf{u}(\mathbf{x}, t)$ is the velocity, $p(\mathbf{x}, t)$ is the pressure, ν is the is the kinematic viscosity, and $\mathbf{F}$ is the sum of all body forces (such as gravity, mean pressure gradient, drag). Pope (2000) and Wilcox (2006) provide a detailed description of the computational methods used for turbulent flows. This study utilises large-eddy simulation (LES), which was initially formulated by Smagorinsky (1963) for simulating atmospheric flows. Deardorff (1970) applied it to the simulation of large Reynolds number flows, and LES has since been an integral tool in industrial and environmental simulation. As resolving the smallest scales in turbulent flows is the most computationally intensive task, LES models these smallest scales instead of explicitly resolving them. This is done by applying a low-pass filter (spatial and temporal averaging) to the Navier–Stokes equations. The effect of these smaller scales on the larger scales is modelled using various sub-grid scale (SGS) models, which are discussed by Pope (2000) in greater detail. Because of its good balance between computational cost and accuracy, LES is the predominant method for simulation of large-scale fluid motions that affect atmospheric flows and bushfires.

The computational modelling of an ember storm at a WUI requires the modelling and incorporation of a few key components: the forest canopy, urban structures, and particles as embers. Each of these components have been studied extensively, but separately, in the existing literature.

2.1 Flow over forest canopies

The density variation of foliage in the forest canopy can be considered as a region of varying drag that affects the wind passing through it. Near the ground, tree trunks are sparsely spaced and generate less drag than the denser foliage near the crowns of trees. Thus the frontal area density, a_f (Pimont et al. 2009) of a forest canopy can be expressed as a function of the height of the forest canopy. Based on the type of vegetation, the profile of a_f can change (Moon et al. 2019). Analytically, the forest canopy can be represented in Equation (2) using a body force term (volumetric drag force) $\overline{f}_{d,i}$, such that, $\overline{f}_{d,i} = -\rho c_d a_f u_i ||\mathbf{u}||$. Here, ρ is the air density, c_d is a drag coefficient, u is the wind velocity in the $i = \{x, y, z\}$ direction. Dupont et al. (2011) performed numerical simulations of a pine forest with deep, sparse trunk space, and characterised the edge flow. Mueller et al. (2014) performed LES of forest canopy flow and could accurately recreate turbulent statistics found in experimental measurements.

2.2 Flow over urban structures

Urban canopies are often simplified and idealised in numerical simulations. A number of numerical studies have simplified the urban environment by means of wall-mounted arrays of cubes (Kanda 2006, Hanna et al. 2002). Bou-Zeid et al. (2009) modeled the campus of Ecole Polytechnique Federale de Lausanne (EPFL) and performed LES to investigate the effect of level of building detail. They found that simple and refined models provided similar mean flow results but different patterns of turbulence. Generally, these urban structures are incorporated into the fluid mesh during the preprocessing stage (discussed in the subsequent sections).

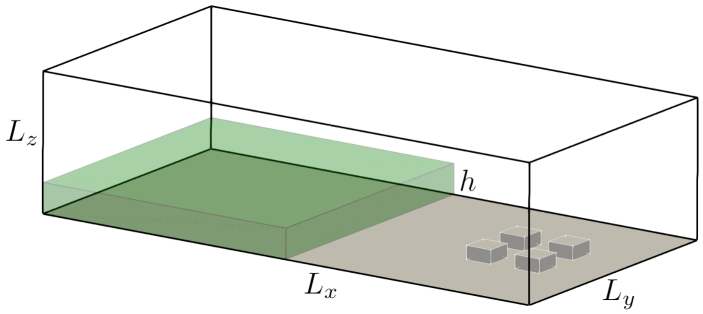

Figure 3. Schematic of the computational domain. L_x, L_y, and L_z are the domain dimensions in $x-y-z$ direction. A uniform forest canopy of height h is modelled from $x = 0$ to $x = L_x/2$. Flow is from the forest canopy towards the cubes.

2.3 Particles (embers) in flow

Particles are taken to be Lagrangian particles in this study. Pollutants in atmospheric flows (Leelőssy et al. 2014), embers in bushfires (Wadhwani et al. 2017), pathogens in respiratory systems (Kleinstreuer & Zhang 2010) are all examples of Lagrangian particles in fluid flow. In the Lagrangian particle transport model, particles follow the equations of motion,

$$m_p \frac{\mathrm{d}\mathbf{u}_p}{\mathrm{d}t} = \mathbf{F}_p(\mathbf{x}_p, t) \tag{3}$$

$$\frac{\mathrm{d}\mathbf{x}_p}{\mathrm{d}t} = \mathbf{u}_p(\mathbf{x}_p, t) \tag{4}$$

where $\mathbf{x}_p$, $\mathbf{u}_p$ and m_p are the position, velocity, and mass of the particle, and $\mathbf{F}_p$ is the sum of forces acting on the particle (such as, lift and drag forces, gravity). Subsequent positions of the particle are found by integrating equation (4). For ember simulation, one-way coupling (fluid flow affects the particles, but the particles do not affect the flow) is sufficient considering that the volume of the fluid domain is much greater than the cumulative volume of the embers (Elghobashi 1994, Kuerten 2016).

3 SIMULATION SETUP

The fluid solver used in this research is the open source spectral element method (SEM) code Nek5000 (Fischer et al. 2022) which solves equations (1) and (2). This solver uses the Galerkin approximation for spatial discretisation, and third-order explicit extrapolation and implicit backward differentiation methods for the non-linear and linear terms, respectively, in the Navier–Stokes equations. The SEM is well-suited for discretising complicated geometries while retaining the high-order accuracy of spectral methods.

h	L_x	L_y	L_z	n_x	n_y	n_z	N	Δx_{gll}	Δy_{gll}	Δz_{gll}	CFL
22 m	400 m	200 m	100 m	32	16	16	9	2.18 m	2.18 m	2.18 m	0.75

Table 1. Summary of the test case parameters. Here, n_x, n_y, and n_z are the total number of macro-elements in the $x-$, $y-$, and $z-$direction respectively. Maximum spacing of GLL points within a macro element can be closely estimated by $\Delta x_{i,gll} = L_{x_i}(\pi/2)(n_{x_i}N)$.

Relevant parameters of the simulation are summarised in Table 1. Houses were represented with cubes, and Gmsh (Geuzaine & Remacle 2009) was used to create a fully hexahedral mesh with a 2×2 array of cubes of size $20 \times 20 \times 10$ m^3. The cubes were placed in a fluid domain of size $400 \times 200 \times 100$ m^3, where a homogeneous forest canopy of height $h = 22$ m was prescribed from $x = 0$ m to $x = 200$ m (Figure 3). The domain is discretised with $32 \times 16 \times 16$ m^3 macro elements, the spacing between which are further divided into a number of GLL points based on a specified polynomial order N (Zahtila et al. 2023). The parameters from *Stand wind sector* case from Dupont et al. (2011) were used to model the canopy. A high-pass filtered (HPF) model was used for the LES, which has been evaluated by Schlatter et al. (2005) for wall-bounded turbulent flows. Separate validation studies performed with this setup showed good agreement with the LES

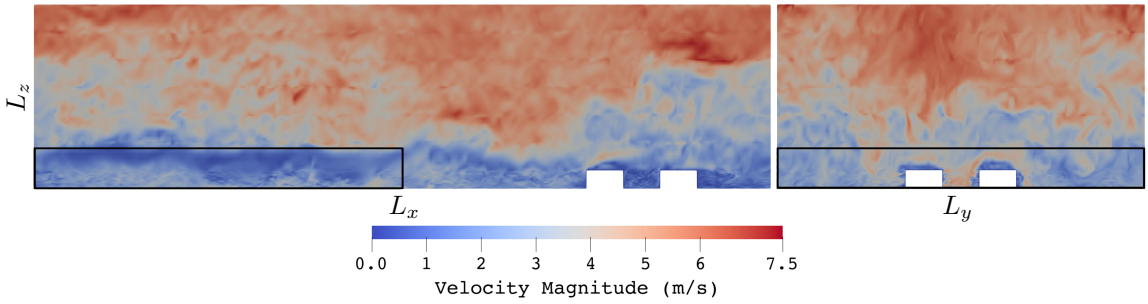

Figure 4. Velocity magnitude contours in the $x-z$ plane (left) and $y-z$ plane (right). The black bounding box demarcates the extent of the forest canopy region. Flow is from left to right (left) and into the page (right). The flow can be seen slowing down within the forest canopy and creating wake structures behind the buildings.

data of Dupont et al. (2011) above the canopy, and overall better agreement with the field experiment data at current grid resolution. Calculation of the second-order statistics requires a longer averaging period and was not done here because the implementation of the other components was prioritised.

The external particle library called 'ppiclF' (Zwick 2019) was modified and integrated with Nek5000 for particle tracking. Particle density was specified as $\rho_p = 500\ \mathrm{kg\,m^{-3}}$ and particles were assumed to have a uniform spherical shape with diameter $d_p = 0.012\ \mathrm{m}$. Periodic boundary conditions were imposed in the $y-$direction for the particles, and any particles exiting the domain in the $x-$direction were deleted. In the absence of a definitive lofting model, the particles were given a phenomenological property that lofted them at height $z_p \propto u_{p,x}^2$, where $u_{p,x}$ is the streamwise velocity of a particle (interpolated from the fluid solution).

The whole setup was run with a no-slip and free-slip boundary condition at the bottom and the top of the domain, respectively, and periodic boundary conditions for the fluid in the $x-$ and $y-$ directions. With a constant temperature assumption, the fluid (air) density was specified as $\rho_f = 1.205\ \mathrm{kg\,m^{-3}}$ and was driven with a constant pressure gradient, $\frac{\mathrm{d}P}{\mathrm{d}x} = -0.004\ \mathrm{Pa\,m^{-1}}$ at constant $CFL = 0.75$. The flow field was allowed to develop for ≈ 400 s. To arbitrarily imitate ember generation, 10,000 particles were injected within the forest canopy at the surface at $x = 100\ \mathrm{m}$, followed by two more injections of 10,000 particles at ≈ 515 s and ≈ 595 s. From the first injection, the particles were tracked for another ≈ 700 s to observe ember accumulation.

4 RESULTS

Cross-sections are taken at $y = 80\ \mathrm{m}$ in the $x-z$ plane and $x = 310\ \mathrm{m}$ in the $y-z$ plane (to ensure that the planes pass through the centre of one row of buildings) to show the contours of velocity magnitude (Figure 4). The drag created by the forest canopy can be seen as a region of low velocity within the bounding box of the canopy, with higher velocity fluid above the canopy. Low velocity regions behind the cubes are also observed. This is expected as the cubes create significant three-dimensional wake structures behind them in a flow (Meng et al. 2021).

Ember accumulation is plotted in Figure 5. Embers can be seen 'creeping' along the ground in long, horizontal structures. These structures were also observed in the numerical simulations of Dupont et al. (2013) and are termed 'aeolian streamers'. The streamers are observed to break up in the clearing between the forest canopy and within the array of the cubes, possibly due to the interaction between the streamers and the wake vortex behind the canopy and the cubes. Figure 6 shows the particles flowing in layers close to the ground around the cubes at the time of second injection. By the end of runtime, the particles settle mostly on the ground and in the gaps between the cubes. It is also noteworthy that while the particles have reasonably heavy accumulation behind the first row of cubes, there are voids behind the last row. The faster flow around the structures carries the particles around, and the particles that get into the wake regions get trapped as they do not have sufficient momentum to escape.

5 DISCUSSION AND CONCLUSIONS

This paper proposed a framework to simulate an ember storm at the wildland-urban interface (WUI). The computational implementation of various components of a WUI was explored, with a phenomenological lifting model applied so that the feasibility of modelling ember storms could be verified. While this phenomenological

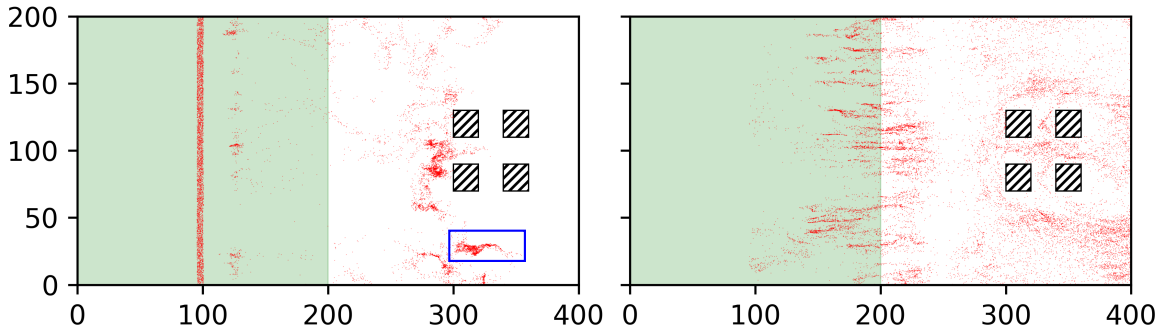

Figure 5. Top down view of ember accumulation at the beginning of second injection (left) and at 700 s (right). A 3D view of the zone bounded by the blue box is presented in Figure 6. The green shaded region demarcates the forest canopy region. Flow is from left to right.

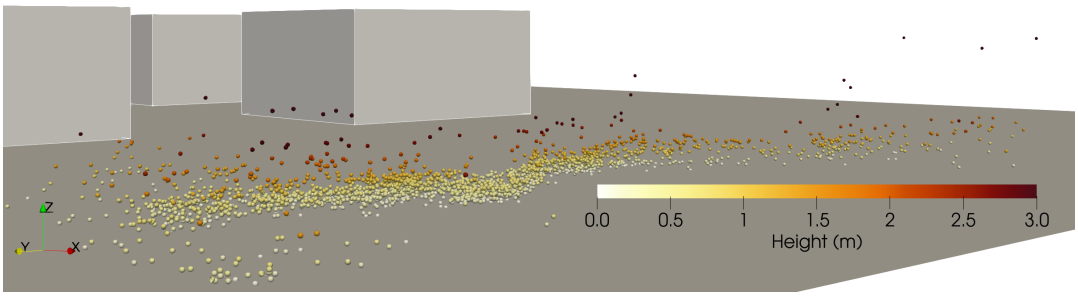

Figure 6. 3D view of embers at the blue bounding box in Figure 5. The elongated horizontal structures resemble those observed in videos (Figure 2) and by Dupont et al. (2013).

model has shown promise, it is also one of the limitations of the proposed framework. In future work, different lifting models from literature will be used to study near-ground particle behaviour. Subsequent work will also investigate the effect of varying wind speed, forest canopy type, and building spacing on the onset of ember storms and patterns of accumulation. Such parametric studies using this framework will facilitate investigation of particular instances of ember storms, as well as pollutant dispersion in forest-to-urban canopy settings.

Acknowledgement

This project received grant funding from the Australian Government, through the Black Summer Bushfire Recovery Grants Program, funding from the ACT Government, with the assistance of resources and services from the National Computational Infrastructure (NCI), which is supported by the Australian Government.
T.S. is supported by a University International Postgraduate Award (UIPA) by UNSW.

References

Blanchi, R. & Leonard, J. (2005), Investigation of bushfire attack mechanisms resulting in house loss in the ACT Bushfire 2003, Technical report, Bushfire Cooperative Research Centre (CRC) Report.

Bou-Zeid, E., Overney, J., Rogers, B. & Parlange, M. (2009), 'The effects of building representation and clustering in large-eddy simulations of flows in urban canopies', *Boundary-Layer Meteorology* **132**, 415–436.

Cruz, M., Sullivan, A., Gould, J., Sims, N., Bannister, A., Hollis, J. & Hurley, R. (2012), 'Anatomy of a catastrophic wildfire: The Black Saturday Kilmore East fire in Victoria, Australia', *Forest Ecology and Management* **284**, 269–285.

Deardorff, J. W. (1970), 'A numerical study of three-dimensional turbulent channel flow at large Reynolds numbers', *Journal of Fluid Mechanics* **41**(2), 453–480.

Douglas, G. B. & Tan, Z. (2005), Integrating site assessment and performance planning outcomes for bushfire prone areas, *in* 'Planning for natural hazards–how we can mitigate impacts? Symposium'.

Dupont, S., Bergametti, G., Marticorena, B. & Simoens, S. (2013), 'Modeling saltation intermittency', *Journal*

of Geophysical Research: Atmospheres **118**(13), 7109–7128.

Dupont, S., Bonnefond, J.-M., Irvine, M. R., Lamaud, E. & Brunet, Y. (2011), 'Long-distance edge effects in a pine forest with a deep and sparse trunk space: In situ and numerical experiments', *Agricultural and Forest Meteorology* **151**(3), 328–344.

Elghobashi, S. (1994), 'Elghobashi, s.: On predicting particle-laden turbulent flows.', *Applied Scientific Research* **52**, 309–329.

Ember attack during bushfire on the Sunshine Coast (2019), *ABC News* .
URL: *https://www.abc.net.au/news/2019-09-09/ember-attack-during-bushfire-on-the-sunshine-coast/11494188*

Fischer, P. F., Lottes, J. W. & Kerkemeier, S. G. (2022), 'NEK - fast high-order scalable CFD', `http://nek5000.mcs.anl.gov`.

Geuzaine, C. & Remacle, J.-F. (2009), 'Gmsh: A 3-D finite element mesh generator with built-in pre- and post-processing facilities', *International Journal for Numerical Methods in Engineering* **79**(11), 1309–1331.

Hanna, S., Tehranian, S., Carissimo, B., Macdonald, R. & Lohner, R. (2002), 'Comparisons of model simulations with observations of mean flow and turbulence within simple obstacle arrays', *Atmospheric Environment* **36**(32), 5067–5079.

Jolly, W. M., Cochrane, M. A., Freeborn, P. H., Holden, Z. A., Brown, T. J., Williamson, G. J. & Bowman, D. M. J. S. (2015), 'Climate-induced variations in global wildfire danger from 1979 to 2013', *Nature communications* **6**, 7537.

Kanda, M. (2006), 'Large-eddy simulations on the effects of surface geometry of building arrays on turbulent organized structures', *Boundary-Layer Meteorology* **118**(1), 151–168.

Kleinstreuer, C. & Zhang, Z. (2010), 'Airflow and particle transport in the human respiratory system', *Annual review of fluid mechanics* **42**, 301–334.

Kuerten, J. (2016), 'Point-particle DNS and LES of particle-laden turbulent flow - a state-of-the-art review', *Flow, Turbulence and Combustion* **97**.

Leelőssy, Á., Molnár, F., Izsák, F., Havasi, Á., Lagzi, I. & Mészáros, R. (2014), 'Dispersion modeling of air pollutants in the atmosphere: a review', *Open Geosciences* **6**(3), 257–278.

Manzello, S. L., Suzuki, S., Gollner, M. J. & Fernandez-Pello, A. C. (2020), 'Role of firebrand combustion in large outdoor fire spread', *Progress in Energy and Combustion Science* **76**, 100801.

McRae, R. (2010), Extreme Fire – a Handbook, Technical report, ACT Government and Bushfire Cooperative Research Centre.

Meng, Q., An, H., Cheng, L. & Kimiaei, M. (2021), 'Wake transitions behind a cube at low and moderate Reynolds numbers', *Journal of Fluid Mechanics* **919**.

Moon, K., Duff, T. & Tolhurst, K. (2019), 'Sub-canopy forest winds: understanding wind profiles for fire behaviour simulation', *Fire Safety Journal* **105**, 320–329.

Mueller, E., Mell, W. & Simeoni, A. (2014), 'Large eddy simulation of forest canopy flow for wildland fire modeling', *Canadian Journal of Forest Research* **44**, 1534–1544.

Owens, D. & O'Kane, M. (2020), 'Final report of the NSW Bushfire Inquiry'.

Pimont, F., Dupuy, J.-l., Linn, R. & Dupont, S. (2009), 'Validation of FIRETEC wind-flows over a canopy and a fuel-break', *International Journal of Wildland Fire* **18**, 775–790.

Pope, S. (2000), *Turbulent Flows*, Cambridge University Press.

Roberts, M., Sharples, J. & Rawlinson, A. (2017), Incorporating ember attack in bushfire risk assessment: a case study of the Ginninderry region, *in* 'Proceedings of the 22nd International Congress on Modelling and Simulation'.

Schlatter, P., Stolz, S. & Kleiser, L. (2005), 'Evaluation of high-pass filtered eddy-viscosity models for large-eddy simulation of turbulent flows', *Journal of Turbulence* .

Smagorinsky, J. (1963), 'General circulation experiments with the primitive equations: i. the basic experiment', *Monthly Weather Review* **91**(3), 99 – 164.

Standards Australia (2018), *AS 3959:2018: Construction of buildings in bushfire-prone areas (Fourth edition): Standards Australia*, AS3959:2018, Standards Australia, Australia.

Wadhwani, R., Sutherland, D., Ooi, A., Moinuddin, K. & Thorpe, G. (2017), 'Verification of a Lagrangian particle model for short-range firebrand transport', *Fire Safety Journal* **91**.

Wilcox, D. (2006), *Turbulence Modeling for CFD*, number 3rd ed., DCW Industries.

Zahtila, T., Lu, W., Chan, L. & Ooi, A. (2023), 'A systematic study of the grid requirements for a spectral element method solver', *Computers & Fluids* **251**, 105745.

Zwick, D. (2019), 'ppiclf: a parallel particle-in-cell library in Fortran', *Journal of Open Source Software* **4**(37), 1400.